Orientation and Morphological Evolution of Catalyst Nanoparticles During Carbon Nanotube Growth

Michael J. Behr, K. Andre Mkhoyan, and Eray S. Aydil*

Department of Chemical Engineering & Materials Science, University of Minnesota, Minneapolis, Minnesota 55455

ARTICLE

ABSTRACT We examined the structure, morphology, and orientation of catalyst nanoparticles used for seeding and growing multiwall carbon nanotubes (MWCNTs) by plasma enhanced chemical vapor deposition in CH_4/H_2 gas mixtures. Iron catalyst nanocrystals are converted to Fe_3C in CH_4/H_2 plasmas and the MWCNTs grow from Fe_3C nanocrystals. Initially faceted and equiaxed catalyst nanocrystals are distorted and elongated significantly once a tubular CNT structure is formed around the catalyst particles. Eventually, catalysts deform into elongated tear-drop shapes. Once this morphology forms, CNT structures produced are straight and have uniform diameters. Surprisingly, the Fe_3C nanocrystals located inside the base of well-graphitized nanotubes do not exhibit a preferred orientation relative to the nanotube axis. Catalyst nanocrystals in a variety of orientations relative to the nanotube axis still produce well-graphitized nanotubes with similar diameters and structures.

KEYWORDS: carbon nanotubes · nanotube orientation · plasma enhanced chemical vapor deposition

A wide-range of potential applications that utilize the unique electronic, mechanical, and optical properties of carbon nanotubes (CNTs) requires precise control of their structure, but such control has not yet been achieved.[1−10] Plasma-enhanced chemical vapor deposition (PECVD), and related CVD processes from CH_4/H_2 gas mixtures using metallic catalyst nanoparticles enable large-scale growth and controlled spatial placement of carbon nanotubes on substrates,[3,11] but these methods always produce a mixture of nanotube structures and sizes. Progress in our fundamental understanding of the atomic-level processes at the catalyst−CNT interface and growth mechanisms has come primarily through careful studies of the structure, phase, and shape of catalyst crystals, from which the nanotubes grow. Both *ex situ* and *in situ* transmission electron microscopy (TEM) techniques and X-ray photoelectron spectroscopy (XPS) have been used to characterize catalyst shape and structure. One surprising finding is that Fe-, Co-, and Ni-based catalysts dynamically change their shape yet remain fully crystalline during high temperature CNT growth by CVD.[12−18] Recently, we used a convergent beam electron diffraction (CBED) technique in the TEM to show that segments of single crystal Fe_3C catalysts located inside the base of multiwall carbon nanotubes (MWCNTs) grown by PECVD were twisted, rotated, and bent[19] by stresses exerted during growth by the graphene walls surrounding the catalyst. These observations suggest that the catalyst nanoparticle and the graphene walls undergo complex dynamic interactions that influence how CNTs grow.

Whether CNTs grow epitaxially on catalyst nanoparticles remains an open issue. If epitaxy is important in CNT growth, orientation of the catalyst nanoparticle and the CNT growth axis should be correlated; observation of an ensemble of CNT-catalyst nanoparticle pairs should show preferred catalyst orientations with respect to the CNT growth axis. It was suggested that decomposition of carbon-containing species and graphite formation may occur on specific crystallographic faces that have high catalytic activity,[20] which may also result in a preferential catalyst orientation relative to the nanotube axis.[21,22] In the case of an Fe_3C nanoparticle catalyst, epitaxial growth of graphene layers from catalyst faces oriented perpendicular to the CNT axis seems unlikely because the symmetry of the two structures, orthorhombic and hexagonal, are incommensurate. However, epitaxy could occur at step edges along the length of the catalyst. Indeed, there are a number of Fe_3C crystallographic planes whose spacing is either equal to, or an integer multiple of, the 0.34 nm CNT wall spacing, and this could lead to epitaxial growth of graphene layers. Specifically, the (001), (110), (002), (030), (220), (004), and (023)

*Address correspondence to aydil@umn.edu.

Received for review April 30, 2010 and accepted August 30, 2010.

Published online September 9, 2010.
10.1021/nn100944n

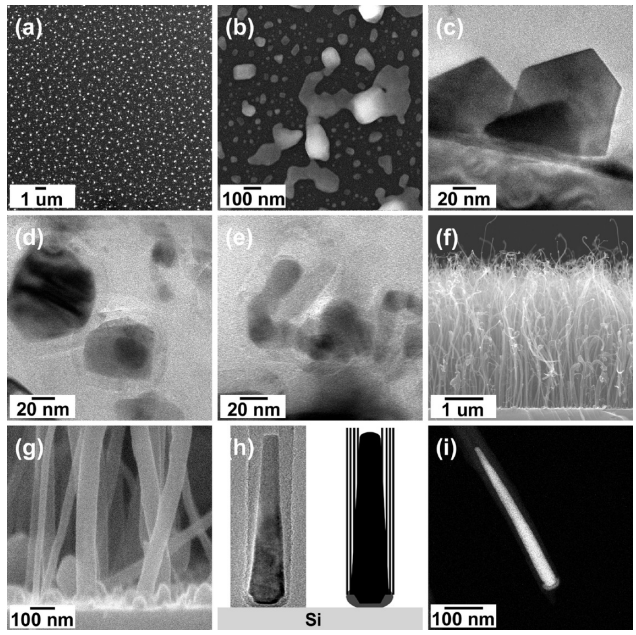

Figure 1. (a) An SEM image of the iron catalyst film that was broken up into small nanometer-sized islands during the hydrogen plasma pretreatment. (b) A magnified view of the faceted iron catalyst islands. (c) Cross-section TEM image of the iron catalyst after pretreatment reveals the faceted nature of the catalyst crystals. (d) Cross-section TEM image of the catalyst film after 5 min of methane plasma exposure (growth conditions) shows deformed catalysts surrounded by ~5 nm thick layer of graphene walls. (e) Cross-section TEM image of an elongated crystal found inside a growing nanotube. (f) Cross-section SEM image of the ~4 μm thick CNT film after 30 min of growth. (g) A magnified view showing the CNT attachment to the substrate as well as catalysts that did not produce CNTs. (h) BF-TEM image (left) of a similar crystal next to a schematic showing pictorially how catalyst crystals remain at the base of the CNT, attached to the substrate. (i) HAADF image of a representative Fe_3C catalyst found inside the base of a MWCNT.

planes could potentially support epitaxial growth. In support of this hypothesis, Wen *et al*. reported that Fe_3C catalyst crystals were preferentially oriented with either their [100] or [101] direction parallel to the nanotube axis. In contrast, other studies highlighted the importance of the initial graphitic seed that forms on the metal in facilitating nanotube growth.[23,24] For example, Marchand *et al*. used field emission microscopy to observe the incremental axial rotation of SWCNTs during growth from nickel nanoparticles,[25] and concluded that this rotation was evidence for growth *via* a screw-dislocation mechanism one carbon dimer at a time, as proposed by Ding *et al*.[26] Herein, we use (S)TEM imaging and diffraction techniques to examine the structure, shape, and orientation of more than 20 Fe_3C catalyst crystals found inside the base of MWCNTs and show that CNTs of similar structure and size grow from catalyst crystals that are in no particular preferred orientation.

RESULTS AND DISCUSSION

Evolution of Structure and Morphology During CNT Growth. Multiwall carbon nanotubes were grown using a radio frequency (13.56 MHz) inductively coupled plasma and iron catalyst through PECVD. Using scanning electron microscope (SEM) and TEM, we examined the structure and morphology of the catalysts at each point throughout the carbon nanotube growth process. Figure 1 panels a and b show low- and high-magnification SEM images of the iron catalyst particles on silicon after pretreatment of the iron film by exposing it to an H_2/Ar plasma. This pretreatment efficiently breaks apart the continuous 10 nm thick film to form nanometer-sized metal islands. A range of metal island sizes was observed, from approximately 10 nm to larger than 100 nm. Although not as evident in the SEM images, the cross-sectional TEM images of the pretreated film (see Figure 1c) clearly show that these metal islands are highly faceted body-centered cubic (BCC) iron crystals. TEM and electron diffraction of these crystals confirm that they are BCC.[27]

After 5 min of H_2/CH_4 plasma exposure, cross-sectional TEM images revealed visible changes to the catalyst crystal shapes and structures (see Figure 1d,e). Through CBED analysis, we found that the initially BCC iron crystals had been transformed into an Fe_3C (cementite) crystal phase (orthorhombic space group *Pnma* No. 62, $a = 0.5008$ nm, $b = 0.4465$ nm, $c = 0.6725$ nm).[19] All catalyst crystals by this point were covered with graphene walls approximately ~5 nm thick, as shown in Figure 1d,e. Catalyst crystals no longer exhibited faceting, and either appeared slightly spherical or deformed from their well-faceted shapes when they were BCC iron. Sun *et al*.[28] showed that CNTs and carbon onions can exert internal pressures up to ~40 GPa, which can cause metal nanocrystals located inside these structures to deform. Such pressures are well above the yield strength of bulk Fe (~140 MPa) and the deformation can be a direct consequence of the enormous pressures that are exerted by the encapsulating graphene walls. The order of catalyst deformation, transformation to Fe_3C, and graphene wall formation is unknown, but the catalysts seemed to lose their facets always after graphene layers had formed around them. Regardless of the order, these events formed the initial seed for the subsequent CNT growth. In fact, some of the catalyst crystals appeared elongated and were found inside short nanotubes, in the very beginning stages of growth. At this initial stage of growth, the nanotubes were typically short (*ca.* 100−150 nm) and highly deformed, exhibiting severe curves or kinks as shown in Figure 1e.

CNTs grew from the Fe_3C catalyst crystals to a length of about 4 μm during plasma exposure for an additional 25 min (see Figure 1f). The majority of CNTs have an average diameter of 29 ± 5 nm, as measured from BF-TEM images; however, larger tubes ~80 nm in diameter that grew from catalyst nanoparticles of different morphologies were also present. As is evident from these SEM images, the straightness of each nanotube varies along its length. Typically, the tips of CNTs are

curled and usually contain large chunks of the catalyst. This curled- and kinked-tip morphology resembles the morphology of the short nanotubes observed during the initial stages of growth (see Figure 1f). This morphology would be expected as CNTs grew longer and this initially deformed section was pushed upward. Toward the base, nanotubes straighten out considerably, as evident in the cross-section SEM image of Figure 1g. Thus, the CNT growth seems to settle into a steady growth process after the deformation and break-up of the initial catalyst particle. This process leaves the tip curled and kinked. Additionally, many catalyst particles did not produce tubes, as is evident by the numerous spherical-shaped graphene-covered catalyst particles in the SEM image shown in Figure 1h. In these cases, we presume that the process that brings additional C atoms to add to the CNT had stopped. Catalyst particles that are completely enclosed in CNTs do not participate in CNT growth. On the basis of this observation we conclude that graphene walls form a diffusion barrier around these catalyst particles and prevent the gas-phase precursor from interacting with the catalyst particle. In contrast, we always observe, on nanoparticles that lead to CNT growth, a section that is free of graphene walls to allow carbon precursor access to the nanoparticle.

Catalyst particles that produced well-graphitized CNTs remained attached to the substrate. In general, CNTs grew *via* a base-growth mode, whereby the catalyst remained attached to the substrate.[7] Our BF-TEM and ADF-STEM images (Figure 1h,i) revealed that the Fe_3C catalysts located inside CNT bases exhibited an elongated tear-drop shape with a constant smooth taper and lengths typically greater than 150−200 nm. Despite a wide distribution of initial catalyst nanoparticle sizes, diameters were very consistent and produced CNTs with a narrow diameter distribution (29 ± 5 nm). These tear-drop shaped catalyst particles, although single crystalline, have combinations of small angle (*ca.* 1−3 deg) misorientations along their axial lengths.[19] The catalyst edges oriented approximately parallel to the axis of the CNT appeared very smooth, while the bases exhibited clear faceting, which is consistent with observations by Begtrup *et al*. who found that Fe catalysts inside CNTs exhibited facets only on the end surfaces exposed to the carbon source.[15] The opposite end of the catalyst usually appeared rounded and often was covered with a layer of graphene. Previous *in situ* microscopy studies have correlated spherical catalyst shape with formation of hemispherical graphene domes during CNT growth.[16] Interior graphene cups observed at various locations along the length of most nanotubes were formed on this rounded end of the catalyst.[27]

Closer examination of the base region of the catalysts, where they were attached to the substrate, revealed that Fe_3C is capped by a ~5 nm thick layer of iron oxide (Fe_xO_y) as determined from EDX and EELS analysis (see Figure 2c,d). Figure 2 panels a and b show

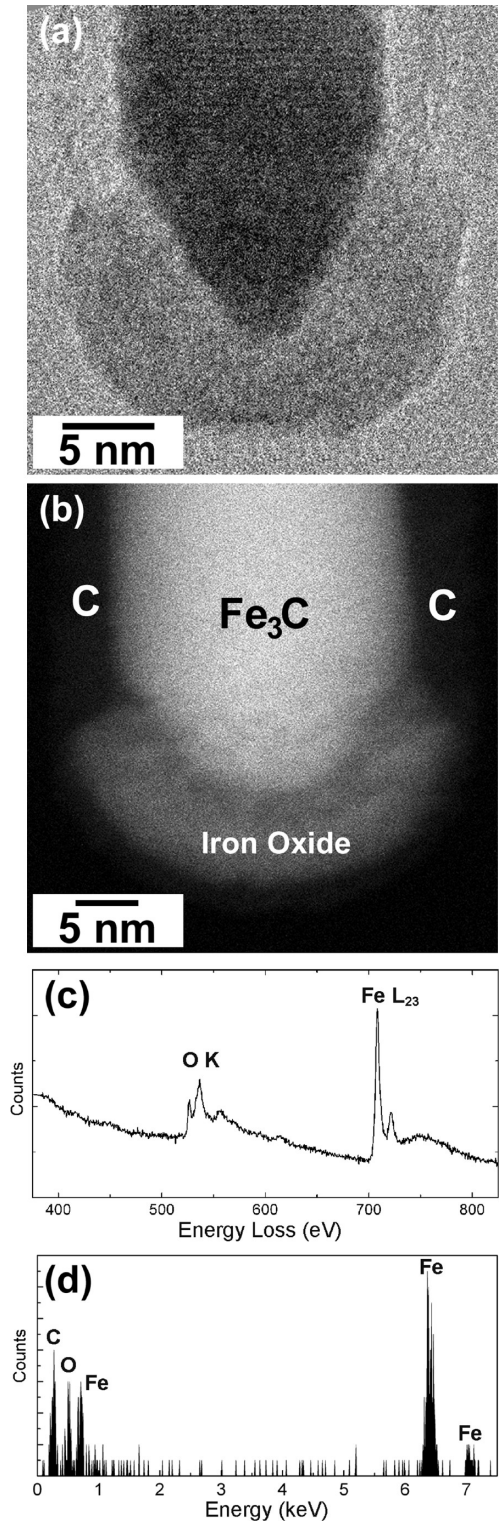

Figure 2. High-resolution (a) BF-TEM and (b) HAADF-STEM images of the base region of two similar catalyst crystals. Both Fe_3C catalysts exhibit clear faceting and are capped by a thin layer of iron oxide. CNT walls do not extend all the way to the base but instead terminate at the iron oxide. (c) EEL and (d) EDX spectra obtained from the catalyst shown in the HAADF image of panel b confirm that the cap at the catalyst base contains iron, oxygen, and carbon.

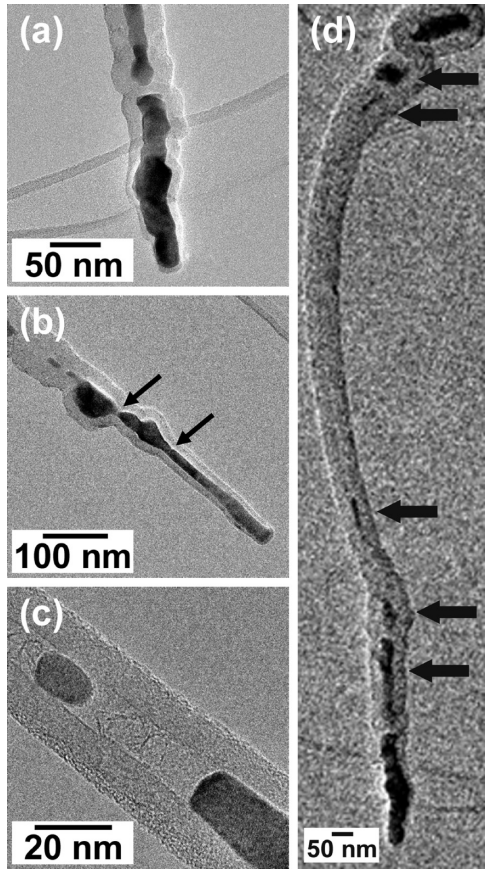

Figure 3. BF-TEM images of catalysts at early stages of CNT growth. (a) A catalyst at the base of a CNT beginning to elongate during the early stages of CNT growth. Adjacent sections of the catalyst are different sizes and are at different orientations. (b) A catalyst observed slightly further along in growth as evident by the more elongated shape. The arrows indicate a point of neck formation, where further growth would cause the catalyst to break in two. (c) A small portion of catalyst that had separated from the base catalyst through this necking process. CBED revealed that the orientation of the two pieces relative to the incident electron beam were identical. (d) An entire nanotube labeled with arrows that show small pieces of catalyst at various points along its length. The majority of catalyst that separates from the base occurs during early stages of growth, and therefore appears at the CNT tip.

BF-HRTEM and HAADF-STEM images of this oxide cap, respectively. The oxide was observed on all catalysts, and existed in both crystalline and amorphous forms. The HAADF-STEM image of Figure 2b, where the intensity is proportional to $Z^{1.7}$ (Z is the average atomic number),[29] clearly shows the different components of the base region. Thin layers of iron oxide were observed by Blank *et al*. on iron carbide catalyst crystals located at the tips of CNFs grown by disproportionation of CO.[30] However, a study by Heresanu *et al*. showed that iron oxides can also form during the cooling step, after CNT growth.[31] In our case, we believe that the oxide is present during the entire growth as a result of oxides not being completely reduced during the pretreatment step or by interaction of the catalyst with the native oxide. The amorphous nature of many of the oxides, as well as the carbon concentration found to exist in the oxide as measured with EELS, supports this conclusion.

Initial Stages of CNT Growth. Next, we examined the early stages of CNT growth to understand how the catalyst morphology changes with the growing nanotube. Figure 3 shows BF-TEM images of Fe_3C catalysts at different stages of CNT growth. Previous *in situ* TEM studies have captured the dynamics of carbon cap formation on Fe_3C catalyst crystals and subsequent cap liftoff from the catalyst during the initial stages of CNT growth.[14] We found that, once a tubular carbon structure formed, the catalyst became severely elongated during growth. For example, Figure 3a shows a BF-TEM image of a catalyst shortly after the tubular structure of a CNT had formed. It has been elongated in the direction of tube growth and consists of adjacent sections that are of different sizes and orientations. The surrounding graphene walls follow the contours of the catalyst, and thus exhibit significant amounts of strain and many kinked sections. This structure reinforces the earlier observation that the curling and bending of the nanotubes, as observed in SEMs, like in Figure 1f, is associated with catalyst deformation and break-up. Figure 3b shows a catalyst inside the base of a CNT that was slightly further along in its growth, as evident by the catalyst's increased elongation. The general shape of the catalyst near the base looks similar to the elongated tear-drop shape of catalysts observed in CNTs grown for 30 min. Large chunks of catalyst are visible inside and farther up the CNT; as more carbon is added from the gas phase, these sections move upward with the growing nanotube. Stresses exerted by the growing nanotube deform the catalyst during growth. Some regions, as indicated by the arrow in Figure 3b experience necking, i.e., plastic deformation as a result of these stresses, which eventually causes the top section of the catalyst to break away from its base. Necking suggests that the catalyst particles experience tensile stresses exerted in the direction parallel to the CNT axis as a result of CNT growth. Figure 3c shows a small section of Fe_3C catalyst that was separated through this process. Continued addition of carbon at the very base of the nanotube after separation caused this small section to move upward approximately 40 nm with the growing nanotube. CBED patterns recorded from this small section and the base revealed that the orientation of the small section was the same as the larger catalyst from which it separated. This process may repeat itself many times as the nanotube grows; the resulting nanotube thus contains numerous Fe_3C catalyst crystals of various lengths from $\sim$10 to $>$100 nm along its length. Figure 3d shows a BF-TEM image of an entire nanotube oriented such that the base of the nanotube is at the bottom of the image. Once detached from the parent catalyst, which remains attached to the substrate, the smaller catalysts inside the growing nanotube no longer participate in the CNT growth process, that is,

they no longer produce graphene layers. We conclude that these catalyst particles do not have access to the carbon source; CNT walls stop the carbon precursor diffusion. Typically, the largest chunks of catalyst are separated from the base catalyst during the initial stages of growth, and thus remain at the CNT tip (see Figure 3d). Because the graphene layers follow the contour of these crystals, the CNT tip usually exhibits many kinks and curves which are not present throughout the rest of the relatively straight CNT, as seen in earlier SEM images (see Figure 1f).

We conclude that our catalysts remain solid and crystalline during growth, based on previous *in situ* observations of CNT growth from crystalline Fe_3C catalysts[12,14] as well as on molecular dynamics simulations of the size-dependent melting behavior of Fe−C particles[32] that indicate catalysts are only completely molten at temperatures above 1200 °C. Yet, we observe that catalysts undergo severe deformations and break apart. As shown in Figure 3, Fe_3C catalyst crystals start to elongate once a tubular CNT structure has formed. At the growth temperature of 800 °C, the thermal expansion coefficient of Fe_3C (4.1×10^{-5} K^{-1})[33] is approximately 1 order of magnitude larger than the thermal expansion coefficient of the surrounding CNT (3×10^{-6} K^{-1}).[34] Additionally, the surrounding CNT walls exert significant internal pressures on the catalysts, ranging from ~20 GPa for single wall to more than 40 GPa for six or more walls.[35] These internal pressures are well above the estimated tensile and compression strengths of ~5 GPa for Fe_3C.[36] The combination of these two effects constrains the catalyst along the CNT axis, elongating the catalyst. The most severe distortions, including neck formation, occur at locations where the number of encapsulating CNT wall is large, that is, locations experiencing the highest internal pressures.

Catalyst Orientation with Respect to the CNT Axis. We determined the orientations of Fe_3C nanocrystals with respect to the CNT growth direction and examined whether there is a preferred orientation between the CNT and the catalyst crystallographic orientation. While the proper description of the growth direction of a SWCNT must include both, the orientation of the CNT relative to the catalyst crystal and the chirality of the CNT, in MWCNTs (>2 walls), the discussion of the chirality of the entire tube becomes meaningless because different walls can have different chirality. Thus, the only remaining meaningful characterization for discussion of CNT growth direction is through the overall orientation of the CNT relative to the catalyst crystal. An unambiguous way to determine the orientation of an Fe_3C crystal located inside a CNT is by searching for and identifying two crystallographic directions of the crystal, each perpendicular to the CNT walls. A double-tilt holder within the TEM enabled tilting of the crystal to multiple zone axes and facilitated this search. The cross product of these two directions yields the catalyst's crystallographic direction that lies along the axis of the CNT (Figure 4). Two SAED patterns used to determine the orientation of a catalyst inside the base of a CNT are shown as an example in Figure 5. In this particular case, the Fe_3C catalyst crystal was tilted to two differ-

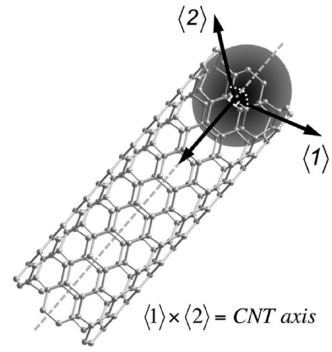

Figure 4. Schematic illustration of the method used to determine the relative orientations of the CNT axis and the catalyst orientation. The catalyst crystal is tilted to multiple zone axes and two crystallographic directions of the crystal, ⟨1⟩ and ⟨2⟩, each perpendicular to the CNT walls, are identified. The cross product of these two directions yields the catalyst's crystallographic direction that lies along the axis of the CNT.

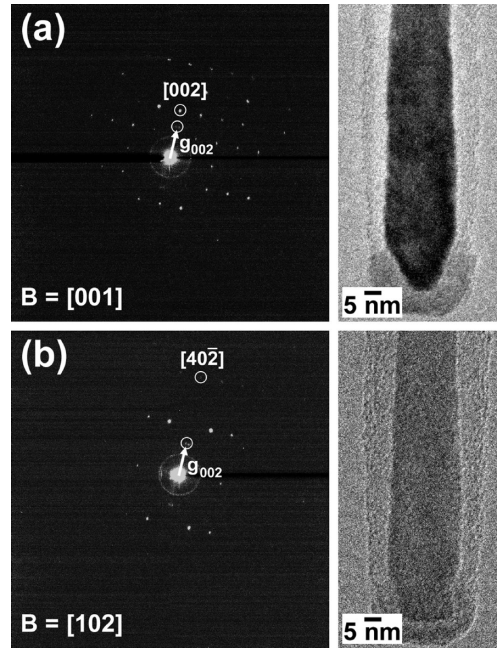

Figure 5. An example illustrating the method used for determining the catalyst orientation relative to CNT axis. First, SAED patterns were obtained from an individual Fe_3C catalyst crystal at two different zone axes, in this example (a) [001] and (b) [102]. BF-TEM images of the same crystal at each orientation are also shown. Two diffraction spots from the surrounding CNT walls are also present in each pattern; one of these spots in each pattern is circled and denoted by its reciprocal lattice vector, $\mathbf{g}_{002}$. This vector, by definition, is perpendicular to the nanotube axis. The Fe_3C crystallographic direction corresponding to the diffraction spot that is in line with this $\mathbf{g}_{002}$ vector is circled and labeled in each pattern, and is thus also perpendicular to the nanotube axis ([002] and [40$\bar{2}$]). The cross product between these two directions yields the orientation of the catalyst along the nanotube axis, [010].

ent zone axes, [001] and [102]. The Fe_3C crystal at each orientation is shown in the BF-TEM images of Figure 5. A selected area electron diffraction (SAED) pattern was recorded at each zone axis such that diffraction from both the catalyst crystal and CNT walls were simultaneously visible. The reciprocal lattice vector, $\mathbf{g}_{002}$, associated with the 002 diffraction spot of the surrounding CNT walls, is perpendicular to the nanotube axis, and is indicated on each pattern. The diffraction spots from the Fe_3C crystal at each orientation that are in line with the diffraction spots from the CNT walls are thus also perpendicular to the nanotube walls. Both diffraction spots are also circled in each SAED pattern. In this example, at the [001] zone axis, the [002] crystallographic direction is perpendicular to the CNT walls, while at the [100] zone axis, the $[40\bar{2}]$ crystallographic direction is perpendicular to the CNT walls. The cross product of these two directions, $[002] \times [40\bar{2}]$, gives the Fe_3C crystallographic direction that is parallel to the CNT axis, [010] in this example. More than 20 Fe_3C crystals located inside the base of CNTs were examined using this method. To our surprise, we did not find a consistent preferred catalyst orientation relative to the nanotube axis. Observed directions relative to the nanotube axis included [001], [031], [114], [010], [100]. Often, however, the CNT $\mathbf{g}_{002}$ vector appeared at a small angle (less than $\sim$5°) relative to Fe_3C diffraction spots at the zone axes visited, and thus a definitive orientation relationship between the catalyst and CNT axis was not even possible. This is only possible if the catalyst was oriented with a much higher-order plane parallel to the CNT axis, or if there was no orientational relationship. Our observed lack of correlation between the catalyst and CNT axis is in contrast to a previous study by Wen *et al*. who found that Fe_3C catalyst crystals were preferentially oriented with either their [100] or [101] direction parallel to the nanotube axis.[21] Their findings appear to be based on a single diffraction pattern for each catalyst, which is correct only if the nanotube axis is oriented perpendicular to the incident electron beam. It is unclear if this criterion was satisfied during their analysis. Moreover, many tubes need to be examined to draw statistically significant conclusions and to establish that the same catalyst orientations are observed multiple times. Observation of a variety of relative CNT and catalyst orientations even within a modest sample of 20 CNTs is surprising and support the conclusion that catalysts with many different orientations with respect to the CNT axis can lead to growth.

Our observation that CNTs of similar structure and size grow from catalyst crystals that are in no particular orientation suggests that the initial CNT seed that forms on the catalyst nanocrystals is key to understanding and controlling CNT growth. It appears that what is necessary for CNT growth is simply a spherical or hemispherical graphene seed on a catalyst, a source of decomposed carbon, and a location where the graphene walls are attached to the catalyst for the C atoms to add. Well-faceted catalyst nanoparticles deform into more rounded shapes as graphene layers form on their surfaces and act as the seeds from which the CNTs begin to grow. If the graphene walls form a nearly perfect and continuous layer on a nanoparticle, access to the carbon source is blocked and the catalyst does not lead to CNT growth. The lack of catalyst orientation suggests that either the initial cylindrical or hemispherical graphene seed can be formed on a variety of Fe_3C crystalline faces, or the catalyst changes its relative orientation after a graphene seed is formed from specific faces. It does not appear that the graphene nanotube walls are necessarily produced in an epitaxial process directly from Fe_3C faces.

Finally, we contrast our findings to studies on SWCNT growth, particularly those where the authors have found that one can alter nanotube orientation and chirality by manipulating the structure and composition of the catalyst particle.[37−40] For example, Chiang *et al*. changed the ratio of Ni to Fe in the catalyst and showed that the atomic spacing in the catalyst affects the epitaxial lattice match with the graphene layers of a CNT and, consequently, the chiral distribution of the resulting SWCNTs.[37] Reich *et al*.[38] and Zhu *et al*.[39] showed that chiral selectivity could occur by control of cap nucleation. For example, Zhu *et al*. showed that the angle of the step edge relative to the growth direction is a key factor in determining chirality.[39] They observed the apparent epitaxial formation of a cone-shaped cap, which transformed into a cylinder as the growth proceeded. However, once the cap lifted off, the particle appeared to change shape, and the CNT walls appeared to originate from a slightly different location. It may be that the initial seed forms epitaxially but the relative orientation of the CNT and the catalyst changes as growth proceeds by the addition of carbon atoms to the existing graphene edges.

There are significant differences in MWCNT and SWCNT growth. For example our catalyst particles receive up to twice as much pressure from the large number of surrounding graphene walls than would catalyst particles surrounded by only a single graphene wall. As a result, the modification of the catalyst crystal and growth of CNT are strongly intertwined. It is entirely possible that any correlation between the catalyst and CNT orientations that may exist during initial nucleation is lost during growth: the epitaxial relation may be important in nucleation of the walls but not during their growth. A combination of our results with those on SWCNTs suggests that the formation of the initial CNT seed on the catalyst is important and the CNT orientation and chirality may be determined at this initial stage. The orientational relation between the catalyst and the CNT(s) may change as the growth proceeds by the addition of carbon atoms to the existing graphene edges. These observations are consistent with the idea

that once an initial seed is formed, all that is needed is a source of carbon to facilitate further growth by addition to existing graphene edges. Thus, when the orientational correlations between the CNTs and the catalyst particles are examined at later stages of the growth one may not find a correlation as discovered herein.

CONCLUSIONS

The growth of CNTs from iron-based catalyst crystals by PECVD was examined *ex situ* with (S)TEM and SEM imaging, EDX and EELS spectroscopy, and diffraction techniques. Although the catalyst film was deposited as BCC iron, CNTs grew during CH_4/H_2 plasma exposure from Fe_3C catalyst crystals. The Fe_3C crystals were located inside the CNT base and remained attached to the substrate. By examining the orientations and structures of the catalysts with TEM at early stages of growth, we determined that the catalyst deforms and breaks apart to yield catalyst particles at the tip and along the length of a CNT. The elongated tear-drop shaped Fe_3C catalyst crystals attached to the substrate, from which the CNTs grew, were found to exist in a variety of different orientations relative to the CNT axis. Despite this, the resulting CNT structures were very similar, and of high quality. This suggests that CNTs do not grow *via* epitaxy on the catalyst particles.

METHODS

Catalyst Nanoparticle Deposition. The iron catalyst was deposited as a 10 nm thick film on native-oxide coated silicon substrates using electron-beam evaporation. Substrates were placed on a resistively heated substrate platen located 25 cm below the planar transformer-coupled plasma coil.[27] Before nanotube growth, the iron catalyst film was heated to 700 °C and exposed to an H_2:Ar (50:5 sccm) plasma maintained with 200 W RF power at 150 mTorr for 15 min to form nanometer-sized metal islands, and to reduce iron oxides present in the catalyst film.

CNT Growth by PECVD. Carbon nanotubes were grown by PECVD from CH_4 and H_2 diluted in Ar in a chamber that was described previously in detail.[41] To grow nanotubes, the temperature was increased to 800 °C after pretreatment and a mixture of CH_4 and H_2 diluted in Ar was introduced into the chamber. A gas mixture of H_2:CH_4:Ar (5:5:68 sccm) was used during this growth step and was chosen on the basis of a previous study,[27] where we found that the addition of a small amount of hydrogen to a methane plasma was necessary to grow well-graphitized straight CNTs with a narrow diameter distribution. These conditions are also typical of many growth protocols that have been reported in the literature.[7]

Electron Microscopy. Characterization of individual CNTs and catalysts, including high-resolution bright field (BF) and high-angle annular dark field (HAADF)-STEM, (S)TEM imaging, electron diffraction (CBED and SAED), energy-dispersive X-ray spectroscopy (EDXS), and electron energy-loss spectroscopy (EELS) was conducted using an FEI Tecnai F-30 (S)TEM with a Schottky field-emission electron gun operated at 300 keV and equipped with a Gatan Enfina spectrometer attached to the bottom of the TEM column. Cross-section TEM samples were made by a standard wedge-polishing technique. For the remainder of the microscopy work, nanotubes were removed from the Si/SiO_2 substrates by sonication in ethanol for 30 s, and then transferred to copper TEM grids coated with a lacey carbon support film.

Acknowledgment. The authors thank Dr. O. Ugurlu for technical support. This material is based upon work supported by the National Science Foundation (NSF) Grant CBET-0613629. This work utilized the University of Minnesota Characterization Facility, which receives partial support from the NSF-NNIN program and capital equipment funding from the NSF through the MRSEC program.

REFERENCES AND NOTES

1. Baughman, R. H.; Zakhidov, A. A.; de Heer, W. A. Carbon Nanotubes—The Route Towards Applications. *Science* **2002**, *297*, 787–792.
2. Dresselhaus, M. S.; Dresselhaus, G.; Charlier, J. C.; Hernandez, E. Electronic, Mechanical and Thermal Properties of Carbon Nanotubes. *Philos. T. Roy. Soc. A* **2004**, *362*, 2065–2098.
3. Melechko, A. V.; Merkulov, V. I.; McKnight, T. E.; Guillorn, M. A.; Klein, K. L.; Lowndes, D. H.; Simpson, M. L. Vertically Alligned Carbon Nanofibres and Related Structures: Controlled Synthesis and Directed Assembly. *J. Appl. Phys.* **2005**, *97*, 041301.
4. Tans, S. J.; Verschueren, A. R. M.; Dekker, C. Room Temperature Transistor Based on a Single Carbon Nanotube. *Nature* **1998**, *393*, 49–52.
5. Trojanowicz, M. Analytical Applications of Carbon Nanotubes: A Review. *Trac-Trend. Anal. Chem.* **2006**, *25*, 480–489.
6. Merkoci, A.; Pumera, M.; Llopis, X.; Perez, B.; del Valle, M.; Alegret, S. New Materials for Electrochemical Sensing VI: Carbon Nanotubes. *Trac-Trend. Anal. Chem.* **2005**, *24*, 826–838.
7. Meyyappan, M. A Review of Plasma Enhanced Chemical Vapour Deposition of Carbon Nanotubes. *J. Phys. D* **2009**, *42*, 213001.
8. Barone, P. W.; Baik, S.; Heller, D. A.; Strano, M. S. Near-Infrared Optical Sensors Based on Single-Walled Carbon Nanotubes. *Nat. Mater.* **2005**, *4*, 86–U16.
9. Granqvist, C. G. Transparent Conductors as Solar Energy Materials: A Panoramic Review. *Sol. Energ. Mater. Sol. C.* **2007**, *91*, 1529–1598.
10. Landi, B. J.; Raffaelle, R. P.; Castro, S. L.; Bailey, S. G. Single Wall Carbon Nanotube Polymer Solar Cells. *Prog. Photovoltaics* **2005**, *13*, 165–172.
11. Ren, Z. F.; Huang, Z. P.; Xu, J. W.; Wang, J. H.; Bush, P.; Siegal, M. P.; Provencio, P. N. Synthesis of Large Arrays of Well-Alligned Carbon Nanotubes on Glass. *Science* **1998**, *282*, 1105–1107.
12. Sharma, R.; Moore, E.; Rez, P.; Treacy, M. M. J. Site Specific Fabrication of Fe Particles for Carbon Nanotube Growth. *Nano Lett.* **2009**, *9*, 689–694.
13. Hofmann, S.; Sharma, R.; Ducati, C.; Du, G.; Mattevi, C.; Cepek, C.; Cantoro, M.; Pisana, S.; Parvez, A.; Cervantes-Sodi, F.; *et al. In Situ* Observation of Catalyst Dynamics During Surface-Bound Carbon Nanotube Nucleation. *Nano Lett.* **2007**, *7*, 602–608.
14. Yoshida, H.; Takeda, S.; Uchiyama, T.; Kohno, H.; Homma, Y. Atomic Scale *in Situ* Observation of Carbon Nanotube Growth from from Solid State Iron Carbide Nanoparticles. *Nano Lett.* **2008**, *8*, 2082–2086.
15. Begtrup, G. E.; Gannett, W.; Meyer, J. C.; Yuzvinsky, T. D.; Ertekin, E.; Grossman, J. C.; Zettl, A. Facets of Nanotube Synthesis: High Resolution Transmission Electron Microscopy Study and Density Functional Theory Calculations. *Phys. Rev. B* **2009**, *79*, 205409.
16. Rodriguez-Manzo, J. A.; Terrones, M.; Terrones, H.; Kroto, H. W.; Sun, L. T.; Banhart, F. *In Situ* Nucleation of Carbon Nanotubes by the Injection of Carbon Atoms into Metal Particles. *Nat. Nanotechnol.* **2007**, *2*, 307–311.
17. Helveg, S.; Lopez-Cartes, C.; Sehested, J.; Hansen, P. L.; Clausen, B. S.; Rostrup-Nielsen, J. R.; Abild-Pedersen, F.;

Norskov, J. K. Atomic Scale Imaging of Carbon Nanofibre Growth. *Nature* **2004**, *427*, 426–429.
18. Schaper, A. K.; Hou, H. Q.; Greiner, A.; Phillipp, F. The Role of Iron Carbide in Multiwalled Carbon Nanotube Growth. *J. Catal.* **2004**, *222*, 250–254.
19. Behr, M. J.; Mkhoyan, K. A.; Aydil, E. S. Catalyst Rotation, Twisting, and Bending During Multiwall Carbon Nanotube Growth. *Carbon* **2010**, *48*, 3840–3845.
20. Jiang, D. E.; Carter, E. A. Carbon Atom Adsorption on and Diffusion into Fe(110) and Fe(100) from First Principles. *Phys. Rev. B* **2005**, *71*, 6.
21. Wen, C. Y.; Huang, C. C.; Cheng, H. Z.; Lu, H. Y. Orientation Relations Between Carbon Nanotubes Grown by Chemical Vapour Deposition and Residual Iron-Containing Catalysts. *J. Mater. Sci.* **2008**, *43*, 123–131.
22. Golberg, D.; Mitome, M.; Muller, C.; Tang, C.; Leonhardt, A.; Bando, Y. Atomic Structures of Iron-Based Single-Crystalline Nanowires Crystallized Inside Multiwalled Carbon Nanotubes as Revealed by Analytical Electron Microscopy. *Acta Mater.* **2006**, *54*, 2567–2576.
23. Yao, Y. G.; Feng, C. Q.; Zhang, J.; Liu, Z. F. "Cloning" of Single-Walled Carbon Nanotubes *via* Open-End Growth Mechanism. *Nano Lett.* **2009**, *9*, 1673–1677.
24. Smalley, R. E.; Li, Y. B.; Moore, V. C.; Price, B. K.; Colorado, R.; Schmidt, H. K.; Hauge, R. H.; Barron, A. R.; Tour, J. M. Single Wall Carbon Nanotube Amplification: *En Route* to a Type-Specific Growth Mechanism. *J. Am. Chem. Soc.* **2006**, *128*, 15824–15829.
25. Marchand, M.; Journet, C.; Guillot, D.; Benoit, J. M.; Yakobson, B. I.; Purcell, S. T. Growing a Carbon Nanotube Atom by Atom: "And Yet It Does Turn". *Nano Lett.* **2009**, *9*, 2961–2966.
26. Ding, F.; Harutyunyan, A. R.; Yakobson, B. I. Dislocation Theory of Chirality-Controlled Nanotube Growth. *Proc. Natl. Acad. Sci. U.S.A.* **2009**, *106*, 2506–2509.
27. Behr, M. J;. Gaulding, E. A.; Mkhoyan, K. A.; Aydil, E. S. Effect of Hydrogen on Catalyst in Carbon Nanotube Growth. J. Appl. Phys. . in press.
28. Sun, L.; Rodriguez-Manzo, J. A.; Banhart, F. Elastic Deformation of Nanometer-Sized Metal Crystals in Graphitic Shells. *Appl. Phys. Lett.* **2006**, *89*, 263104.
29. Nellist, P. D.; Pennycook, S. J. The Principles and Interpretation of Annular Dark-Field *Z*-Contrast Imaging. *Adv. Imaging Electron. Phys.* **2000**, *113*, 147–203.
30. Blank, V. D.; Kulnitskiy, B. A.; Batov, D. V.; Bangert, U.; Gutierrez-Sosa, A.; Harvey, A. J. Electron Microscopy and Electron Energy Loss Spectroscopy Studies of Carbon Fiber Formation at Fe Catalysts. *J. Appl. Phys.* **2002**, *91*, 1657–1660.
31. Heresanu, V.; Castro, C.; Caqmbedouzou, J.; Pinault, M.; Stephan, O.; Reynaud, C.; Mayne-L'Hermite, M.; Launois, P. Nature of the Catalyst Particles in CCVD Synthesis of Multiwalled Carbon Nanotubes Revealed by the Cooling Step Study. *J. Phys. Chem. C* **2008**, *112*, 7371–7378.
32. Ding, F.; Bolton, K.; Rosen, A. Iron-Carbide Cluster Thermal Dynamics for Catalyzed Carbon Nanotube Growth. *J. Vac. Sci. Technol., A* **2004**, *22*, 1471–1476.
33. Wood, I. G.; Vocadlo, L.; Knight, K. S.; Dobson, D. P.; Marshall, W. G.; Price, G. D.; Brodholt, J. Thermal Expansion and Crystal Structure of Cementite, Fe_3C, between 4 and 600 K Determined by Time-of-Flight Neutron Powder Diffraction. *J. Appl. Crystallogr.* **2004**, *37*, 82–90.
34. Li, C. Y.; Chou, T. W. Axial and Radial Thermal Expansions of Single-Walled Carbon Nanotubes. *Phys. Rev. B* **2005**, *71*, 235414.
35. Sun, L.; Banhart, F.; Krasheninnikov, A. V.; Rodriguez-Manzo, J. A.; Terrones, M.; Ajayan, P. M. Carbon Nanotubes as High-Pressure Cylinders and Nanoextruders. *Science* **2006**, *312*, 1199–1202.
36. Tomota, Y.; Lukás, P.; Neov, D.; Harjo, S.; Abe, Y. R. *In Situ* Neutron Diffraction During Tensile Deformation of a Ferrite-Cementite Steel. *Acta Mater.* **2003**, *51*, 805–817.
37. Reich, S.; Li, L.; Robertson, J. Control of the Chirality of Carbon Nanotubes by Epitaxial Growth. *Chem. Phys. Lett.* **2006**, *421*, 469–472.
38. Zhu, H. W.; Suenaga, K.; Wei, J. Q.; Wang, K. L.; Wu, D. H. *J. Cryst. Growth* **2008**, *310*, 5473–5476.
39. Chiang, W. H.; Sankaran, R. M. Linking Catalyst Composition to Chirality Distrbutions of as-Grown Single-Walled Carbon Nanotubes by Tuning Ni_xFe_{1-x} Nanoparticles. *Nat. Mater.* **2009**, *8*, 882–886.
40. Harutyunyan, A. R.; Chen, G. G.; Paronyan, T. M.; Pigos, E. M.; Kuznetsov, O. A.; Hewaparakrama, K.; Kim, S. M.; Zakharov, D.; Stach, E. A.; Sumanasekera, G. U. Preferential Growth of Single-Walled Carbon Nanotubes with Metallic Conductivity. *Science* **2009**, *326*, 116–120.
41. Agarwal, S.; Takano, A.; van de Sanden, M. C. M.; Maroudas, D.; Aydil, E. S. Abstraction of Atomic Hydrogen by Atomic Deuterium from an Amorphous Hydrogenated Silicon Surface. *J. Chem. Phys.* **2002**, *117*, 10805–10816.